

Multiband superconducting state and Lifshitz transition in $V_{0.7}Re_{0.3}Se_2$ at high pressureCan Tian,¹ Xiaoli Huang ^{1,*} Yiping Gao,¹ Fubo Tian ¹ Min Liang,¹ Yuqiang Fang,^{2,†} Fuqiang Huang,² and Tian Cui^{3,1,‡}¹State Key Laboratory of Superhard Materials, College of Physics, Jilin University, Changchun 130012, China²State Key Laboratory of High Performance Ceramics and Superfine Microstructure, Shanghai Institute of Ceramics, Chinese Academy of Sciences, Shanghai 200050, China³School of Physical Science and Technology, Ningbo University, Ningbo 315211, China

(Received 1 June 2023; revised 13 October 2023; accepted 31 October 2023; published 17 November 2023)

Tracking the mechanism behind the unconventional superconductors has been recognized as a great challenge and remains one of the major problems in multifields. Layered transition metal dichalcogenides (TMDs) offer an important platform for exploring novel physics. Here, we have discovered that the synergetic Re doping and pressure effect on VSe_2 prompts the appearance of multiband superconductivity at 11.5 GPa with $T_c \sim 3.8$ K. By the application of external magnetic fields, this superconducting state is signified by the unusual temperature-upper critical field relationship and the upper critical field characteristic with an upward curvature in the whole pressure range of 12.4–72.7 GPa. The clear experimental evidence of a dominant carrier-type change from electron to hole strongly supports the Lifshitz transition at 37.3 GPa. The tendency of $T_c(P)$ with a dome shape derives from the structural transition and Lifshitz transition at 20.9 and 37.3 GPa, respectively. The first-principles calculations further clarify that the $V-3d$, $Re-5d$, and $Se-4p$ orbitals at the Fermi level contribute to the transformation from the single-band into multiband superconductivity. This work reports the multiband superconductivity in TMDs materials via pressure treatment.

DOI: [10.1103/PhysRevB.108.L180507](https://doi.org/10.1103/PhysRevB.108.L180507)

As an exotic quantum phenomenon, superconductivity has attracted extensive attention for more than a century [1–3]. Exploring new superconducting materials and unveiling the secrets of superconducting pairing have been the main driving force behind the continuous effort in superconductivity research due to the scientific challenges and technological prospects. To date, the most promising stable high-temperature superconducting systems seem to be layered cuprates [4], iron-based superconductors [5], and hydride superconductors [6–8]. Different types of superconductors include the single-band [9], multiband [10], s -wave [11], p -wave [12], and d -wave superconductors [13]. Among the various superconducting states, multiband superconductors have triggered the possible unexpected superconducting mechanism because of intriguing properties and novel phenomena different from single-band s -wave superconductors, for example, the record high superconducting transition temperature (T_c) in conventional superconductor MgB_2 [14] and the observation of the inverse isotope effect in iron-based multiband superconductor $[(Ba, K)Fe_2As_2]$ [15].

It has been well established that superconductivity in electronic correlated systems can be determined by the degrees of freedom of lattice, charge, orbital, and spin, all of which can be manipulated by external stimuli [16–19]. One of the important directions to induce new superconducting states is through doping or substitution, particularly for cuprates and iron-based superconductor systems [20,21]. The doping

method has created many exotic physical properties, such as double-dome superconductivity [22], non-Fermi-liquid behavior [23], and anomalous Hall effect [24]. These findings have renewed interest in investigating the manifestation and mechanisms of superconductivity in the doped system. On the other hand, pressure has played a key role in the generation and control of the superconducting states by tuning the crystal and electronic structures [25,26]. For example, the application of high pressure on $HfSe_2$ induced dimensional transformation from a two-dimensional layered structure to an isotropic three-dimensional network structure [27]. Studies on $1T-Fe_{0.05}TaS_2$ indicated that with increasing pressure, the antiferromagnetism state was suppressed and a superconducting state appeared [28]. Obviously, pressure has constantly broadened our perceptions of the structural and electronic properties of transition metal dichalcogenides (TMDs), and more intriguing phenomena in layered materials are highly expected through pressure regulation. In this regard, it is greatly attractive to achieve new superconducting states in the doped TMDs at high pressures.

The synergetic doping and pressure effect could modulate the Fermi surface topology, which is significant for discovering new quantum matters. To this end, here we have chosen doped VSe_2 (namely $V_{0.7}Re_{0.3}Se_2$) as the target, considering the binary $1T-VSe_2$ exhibiting unique electronic properties with both the charge density wave (CDW) phase and the superconducting state under pressure, as well as being demonstrated to be an electron-dominated single-band compound [29]. Intriguingly, an uncommon multiband superconducting behavior is observed in $V_{0.7}Re_{0.3}Se_2$ at high pressure. The present work opens an avenue for finding more unique superconducting states in the TMDs materials.

*Corresponding author: huangxiaoli@jlu.edu.cn†Corresponding author: fangyuqiang@mail.sic.ac.cn‡Corresponding author: cuitian@nbu.edu.cn

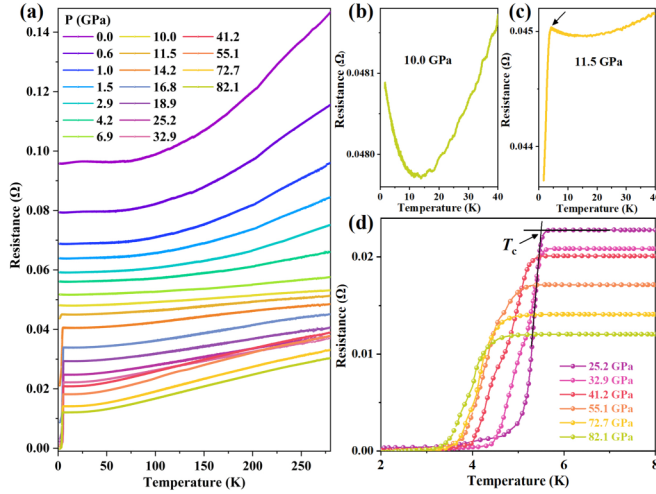


FIG. 1. Temperature dependence of electrical resistance in $V_{0.7}Re_{0.3}Se_2$ sample (no. 1) under high pressures. (a) The plot of resistance as a function of temperature up to 82.1 GPa. (b) Enlarged views of the resistance versus temperature below 40 K at 10 GPa. (c) The magnified curve of the resistance versus temperature below 40 K at 11.5 GPa. The significant resistance drop was indicated by the arrow at $T_c \sim 3.8$ K. (d) The low-temperature resistance in the pressure range of 25.2–82.1 GPa, displaying the superconducting transitions. T_c is defined as the intersection point between two straight lines below and above the superconducting transition.

$V_{0.7}Re_{0.3}Se_2$ crystals were synthesized through a high-temperature solid-state reaction method. The details about the experimental and computational methods are provided in the Supplemental Material [30] and Refs. [31–40]. After synthesizing the target sample $V_{0.7}Re_{0.3}Se_2$, we performed electrical resistance measurements on the $V_{0.7}Re_{0.3}Se_2$ sample (no. 1). Figure 1(a) presents typical plots of temperature versus resistance for different pressures from 0 to 82.1 GPa. Over the investigated pressure range, $R(T)$ displayed metallic behavior, as observed at ambient pressure. With the increase of pressure, the resistance was progressively reduced, and resistance upturn below 10 K was considered to be the Kondo effect caused by the localized magnetic moments of interlayer V ions to the scattering of conduction electrons [Fig. 1(b)]. As the external magnetic field increases, the phenomenon of low-temperature upturn in resistance still can be detected [Fig. S3 [30]]. Above 10 GPa, this special resistance upturn contributed by the Kondo effect was suppressed [Fig. S4 [30]]. Accompanying the collapse of the Kondo effect order, we found a sudden drop of resistance below ~ 3.8 K at 11.5 GPa [Fig. 1(c)], which became pronounced upon further compression. A zero-resistance state was observed at 25.2 GPa, indicating a possible superconducting transition [Fig. 1(d)]. T_c increased rapidly with pressure and maintained a constant value of ~ 5.5 K from 20.9 to 35.5 GPa, followed by a slow decrease rate with 0.02 K/GPa up to the highest pressure. Another sample (no. 2) attained reproducible experimental results in the studied pressure range of 0–78.1 GPa [Fig. S5 [30]].

The existence of pressure-induced superconductivity is further verified by measuring the resistance curves around T_c at different magnetic fields. We have presented the field

dependence of $R-T$ curves in Figs. S6–S8 [30]. At all pressures, T_c was gradually suppressed with increasing magnetic fields, which gave complimentary evidence of the superconducting transition above 11.5 GPa. We determined T_c by using the intersection point between two straight lines below and above the superconducting transition from the $R(T)$ curves [Fig. S9 [30]], and summarized the upper critical field values [$\mu_0 H_{c2}(T)$] for various pressures in Fig. 2. Strikingly, the temperature-dependent $\mu_0 H_{c2}(T)$ of $V_{0.7}Re_{0.3}Se_2$ deviated from the single-band model-based conventional Werthamer-Helfand-Hohenberg (WHH) formula [41] [Fig. 2(b) and Fig. S10 [30]]. Although the unconventional superconductivity is recognized by surpassing the expected WHH limit, alternative models should also be taken into account. We found that the modified Ginzburg-Landau (GL) formula $\mu_0 H_{c2}(T) = \mu_0 H_{c2}(0) \times [(1-t^2)/(1+t^2)]^m$ ($t = T/T_c$) [42], where m is a constant, fitted these $\mu_0 H_{c2}(T)$ data well. The corresponding fitted parameters obtained at different pressures are presented in Fig. 2(c). This unusual pressure and temperature dependence of the $\mu_0 H_{c2}(T)$ curve characterized by a pronounced upward positive curvature (or kink) was also observed in other types of superconductors [43,44]. The kink of $\mu_0 H_{c2}(T)$ may reflect multiband superconductivity, which has been confirmed in other layered superconductors, such as MgB_2 [45] and $FeSe$ [46]. More evidence for this multiband superconductivity could be found from the Hall resistance measurements and calculated band structures in the below parts. This is a successful example that the multiband superconducting state was induced into the doped TMDs by the regulation of the pressure.

In order to compare the data with existing models, it is very necessary to determine the simplified critical field $h^*(t) = \mu_0 H_{c2} / [T_c \times (d\mu_0 H_{c2} / dT)|_{T=T_c}]$, where $t = T/T_c$ represents the normalized temperature [Fig. 2(d)]. All the $\mu_0 H_{c2}(T)$ curves collapse on a single function $h^*(t)$, indicating that the functional behavior does not change with pressure. We also traced the universal $h^*(t)$ models for a spin-singlet s -wave superconductor with orbital limited upper critical field $\mu_0 H_{c2}^{orb} = 0.72 T_c (d\mu_0 H_{c2} / dT)|_{T=T_c}$ [41], and a polar p -wave superconductor of $h^*(0) \sim 0.85$ [47]. The experimental $h^*(t)$ apparently deviated from the standard spin-singlet behavior predicted by WHH theory and the calculated maximum value for a polar p -wave state. Notably, the fact that our $h^*(t)$ data matched the d -wave model function better [48], but there were minor discrepancies below $t \sim 0.4$. We have summarized the derived superconducting critical parameters in Table S3 [30]. The spin-triplet p -wave and single-band conventional WHH models were not sufficient to interpret the $\mu_0 H_{c2}(T)$ data in pressurized $V_{0.7}Re_{0.3}Se_2$. A similar situation exists for the $h^*(t)$ data reported for the superconductor Bi_2Se_3 [49]. The Bardeen-Cooper-Schrieffer (BCS) theory gave the relationship $\mu_0 H_{c2}(0) \propto T_c^2$ for the clean limit superconductor [50], whereas for $V_{0.7}Re_{0.3}Se_2$ below 30 GPa, $\mu_0 H_{c2}(0)$ decreased nearly by a factor of 1.8, but T_c increased by 44% [Fig. 2(e)]. At higher pressures, both $\mu_0 H_{c2}(0)$ and T_c decreased concurrently. This phenomenon further hinted at the noticeable change of the Fermi surface for the high-pressure superconducting state around 30 GPa. In order to better understand the superconducting properties, we extracted the Fermi velocity (v_F), which is closely related to the Fermi surface, using

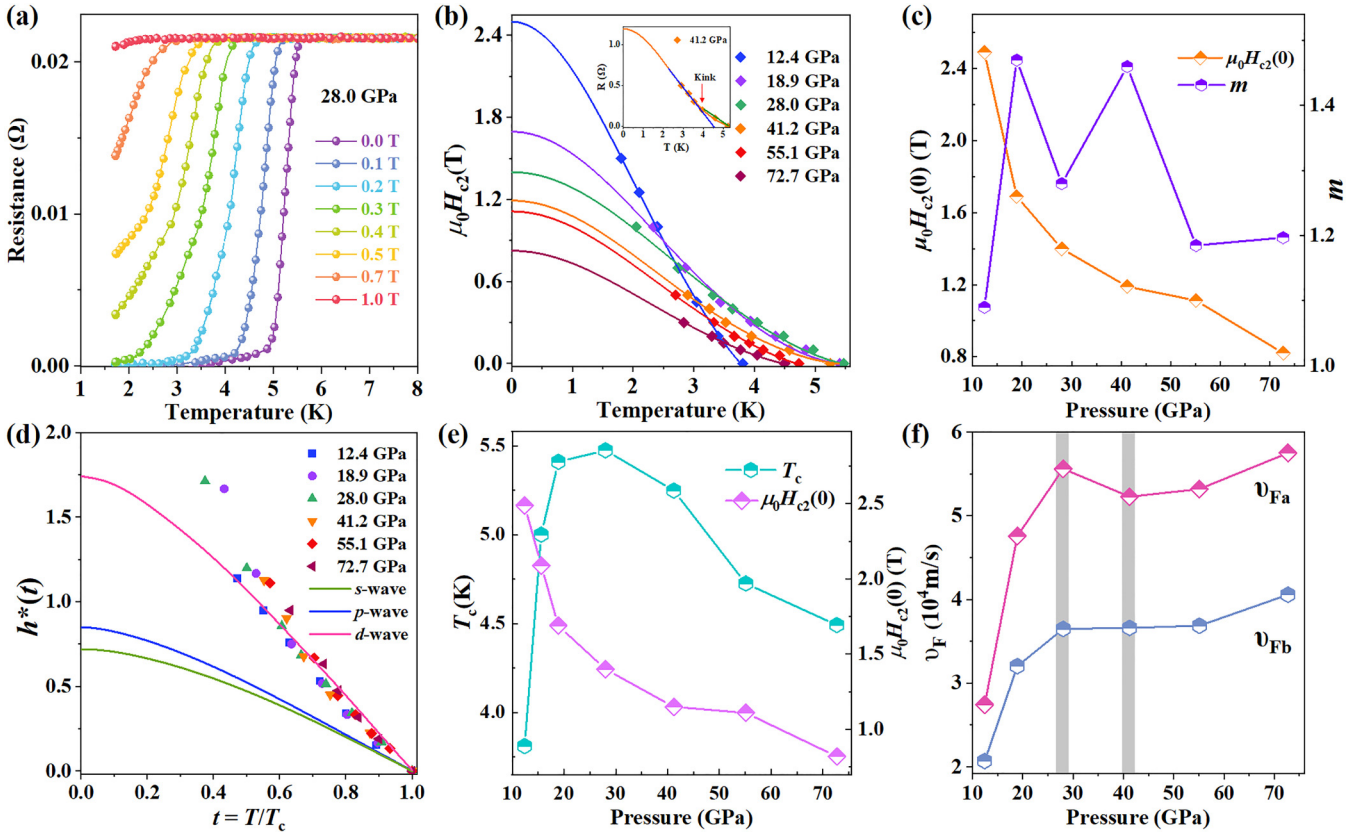


FIG. 2. Upper critical field for $V_{0.7}\text{Re}_{0.3}\text{Se}_2$ (no. 1) under various pressures. (a) Temperature-dependent resistance under various magnetic fields up to 1.0 T at 28.0 GPa. (b) The upper critical field $\mu_0 H_{c2}$ versus T curves at different pressures. The solid lines are fitted by the modified GL formula. The inset shows the position of the kink at 41.2 GPa, indicated by an arrow. (c) The $\mu_0 H_{c2}(0)$ and fitted exponent m at different pressures. (d) The reduced upper critical field $h^*(t)$ as a function of reduced temperature $t = T/T_c$. The green, blue, and pink solid lines denote model calculations for an orbital limited s -wave superconductor, a polar p -wave state, and the d -wave state, respectively. (e) The evolution of upper critical field $\mu_0 H_{c2}(0)$ and T_c under pressure. (f) The Fermi velocity (v_F) as a function of pressure. v_F was determined by the relation $S = -(d\mu_0 H_{c2}/dT)|_{T_c}/T_c \propto 1/v_F^2$ from Fig. S12 [30].

the relationship $S = -(d\mu_0 H_{c2}/dT)|_{T_c}/T_c \propto 1/v_F^2$ [48]. Since each $\mu_0 H_{c2}(T)$ curve has two branches, we have obtained the different slopes ($d\mu_0 H_{c2}/dT$) of the upper kink temperature (K_{above}) and the lower kink temperature (K_{below}) via linear fitting $\mu_0 H_{c2}(T)$, respectively [Fig. S11 [30]]. Then, we can estimate the S_a and S_b of the two respective branches [Fig. S12 [30]]. Finally, the calculated v_F at different pressures is shown in Fig. 2(f). One can see that v_{Fa} first increased at a large rate but decreased at a smaller rate above 30.0 GPa, while v_{Fb} increased slightly between 30.0 and 41.2 GPa. These phenomena manifested the possible changes of the Fermi surface. Altogether, $V_{0.7}\text{Re}_{0.3}\text{Se}_2$ not only exhibited unusual superconductor behavior but also possessed multiband characteristics.

To further prove the peculiar multiband superconducting feature in $V_{0.7}\text{Re}_{0.3}\text{Se}_2$, we have carried out high-pressure Hall effect measurements by sweeping the external magnetic field (H) parallel to the c axis from -7 T to $+7$ T. Figure 3 displays the Hall resistance R_{xy} as a function of H for different pressures at 10 K. During the compression process, the morphology of the sample remained intact without the fracture phenomenon [Fig. S13 [30]]. As can be seen in Fig. 3(a), the $R_{xy}(H)$ curve at 0.5 GPa exhibited linear character with a negative slope at the low field range (0–3 T), but it became nonlinear in the high field region, manifesting that both

electron and hole carriers contribute to the electrical transport properties. This nonlinear behavior also proves the multiband characteristic after Re atom doping into the original binary $1T\text{-VSe}_2$. We have extracted the Hall coefficient (R_H) from Hall resistance $R_{xy}(H)$ below 3 T at different pressures and established the pressure dependence of R_H [Fig. 3(b)]. The slope of $R_{xy}(H)$ first showed a decreasing trend with increasing pressure and then increased upon further compression above 37.3 GPa. R_H was overall negative below 37.3 GPa, reflecting that the electron carriers were dominant. Moreover, the value of R_H changed from negative to positive at ~ 37.3 GPa, suggesting a dominant carrier-type inversion from electron (n type) to hole (p type). The sign variation in R_H with pressure implied that the Fermi surface of $V_{0.7}\text{Re}_{0.3}\text{Se}_2$ underwent a possible significant reconstruction and could be regarded as a sign of the Lifshitz transition, consistent with the above conclusions from the data of critical magnetic fields.

To investigate whether the observed uncommon superconducting state is associated with the pressure-induced crystal structural changes, we performed high-pressure synchrotron x-ray diffraction (XRD) measurements on the $V_{0.7}\text{Re}_{0.3}\text{Se}_2$ sample under different pressures. As shown in Fig. 4, all diffraction peaks gradually shifted to higher angles with increasing pressure, and the patterns can be nicely indexed

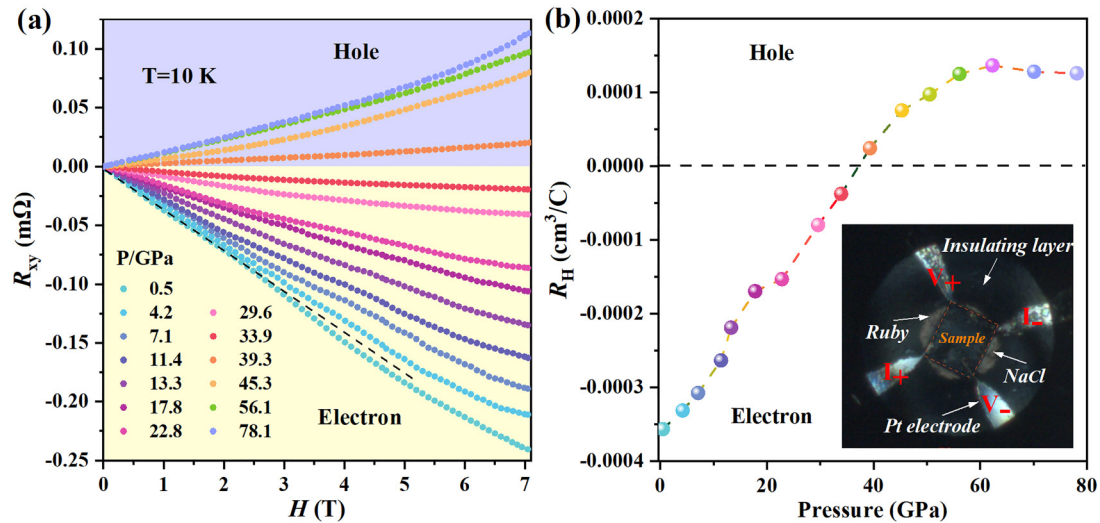


FIG. 3. Hall effect of $V_{0.7}Re_{0.3}Se_2$ (no. 2) under high pressures. (a) Hall resistance (R_{xy}) as a function of the magnetic field at 10 K under various pressures. (b) The pressure-dependent Hall coefficient R_H of $V_{0.7}Re_{0.3}Se_2$. The inset shows the photograph of $V_{0.7}Re_{0.3}Se_2$ using the Van der Pauw method for high-pressure Hall measurements.

with the hexagonal $P\bar{3}m1$ phase below 21.1 GPa [Fig. S14(a) [30]]. At 21.1 GPa, a new diffraction peak at $\sim 17^\circ$ appeared, indicating the emergence of a structural phase transition. The new phase could be possibly determined as the monoclinic $1T'$ structure with the $C2/m$ space group [Fig. S14(b) and Table S4 [30]]. The lattice parameters and unit cell volume for $V_{0.7}Re_{0.3}Se_2$ as a function of pressure

are presented in Figs. 4(b) and 4(c). The third-order Birch-Murnaghan equation of state (EOS) [51] fitting to the data gave ambient-pressure bulk modulus $B_0 = 43.5(9)$ GPa, its first-order derivative $B'_0 = 8.6(3)$, and ambient-pressure volume $V_0 = 59.8 \text{ \AA}^3$ for the $1T$ phase, and $B_0 = 99.5(7)$ GPa, $B'_0 = 3.3(2)$, and $V_0 = 56.9 \text{ \AA}^3$ for the high-pressure $1T'$ phase. Furthermore, no significant volume change was

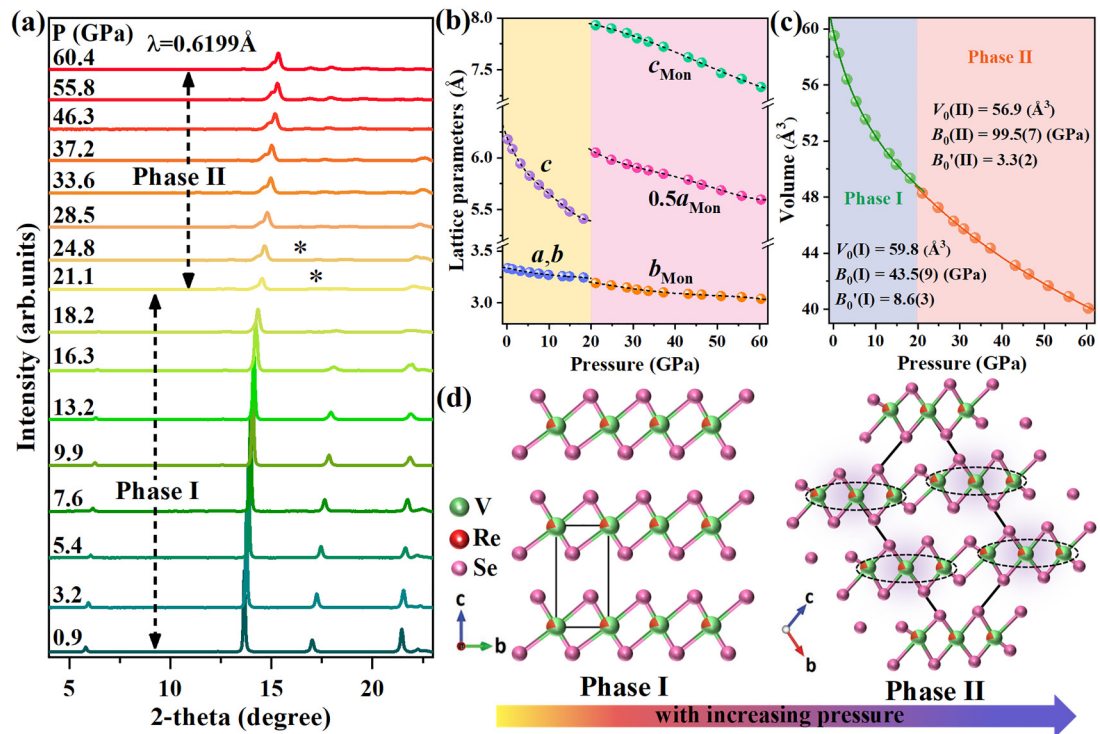


FIG. 4. Structural information for $V_{0.7}Re_{0.3}Se_2$ at high pressures. (a) X-ray diffraction patterns were collected in the pressure range of 0.9–60.4 GPa. Black asterisks mark the emergence of new Bragg peaks. (b), (c) Pressure dependences of the lattice parameters and unit cell volume. (d) Schematic crystal structure of $V_{0.7}Re_{0.3}Se_2$ before and after phase transition, labeled as phase I and phase II, respectively. The unit cells are represented by the black rectangular boxes.

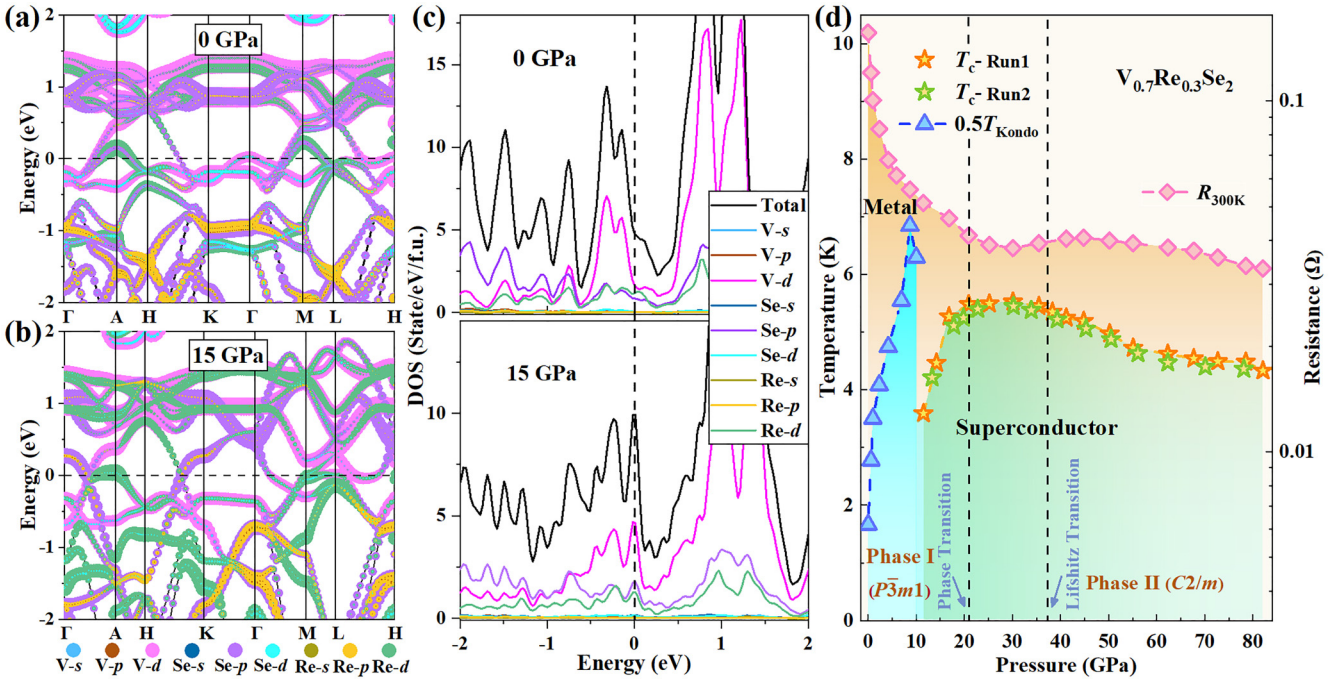


FIG. 5. Electronic properties and temperature-pressure phase diagrams of $V_{0.7}Re_{0.3}Se_2$ (no. 1). (a), (b) Electronic band structure of $V_{0.7}Re_{0.3}Se_2$ in the $P\bar{3}m1$ phase at different pressures. (c) Total and projected electronic density of states at ambient pressure and 15 GPa. (d) Structural and electronic phase diagram of $V_{0.7}Re_{0.3}Se_2$. Resistances at 300 K have been plotted on the logarithmic scale (labels on the right axis). The T_c and T_{Kondo} are extracted from electrical resistance measurements. The vertical dashed lines signify a guide to the electronic state and structural phase transition, respectively.

detected during the transition from the $1T$ to the $1T'$ phase, so this transition was considered as a second-order structural transition. As shown in Fig. 4(d), we exhibited the structure schematic diagram of the $1T$ and $1T'$ phases to clearly demonstrate the pressure-induced structural transition. Upon compression, the $1T$ phase distorted into the high-pressure $1T'$ phase, and transition metal atoms were displaced from the octahedron centers to form trimers, resulting in a 3×1 periodic lattice distortion. We found that the emergence of superconductivity (11.5 GPa) was earlier than the structural transformation (21.1 GPa). Therefore, we consider that the unusual multiband superconducting state does not originate from the crystal structural changes of $V_{0.7}Re_{0.3}Se_2$, but is related to electronic structural changes of the Fermi surface.

Electronic properties of $V_{0.7}Re_{0.3}Se_2$ were further investigated by density functional theory (DFT) calculations to figure out the origin of superconductivity under pressures. Figures 5(a) and 5(b) show the electronic structure of $V_{0.7}Re_{0.3}Se_2$ at different pressures. At ambient pressure, $V_{0.7}Re_{0.3}Se_2$ was metallic with hole pockets at A , Γ , M , and electron pockets between Γ - A , Γ - M , and L - H . The coexistence of electron and hole pockets at the Fermi surface indicated the multiband characteristics of $V_{0.7}Re_{0.3}Se_2$, which was consistent with the Hall effect experimental results. In Figs. 5(a) and 5(b), we can see that the bottom of the conduction band (CB) mainly originates from the V - d and Re - d orbitals, and the top of the valence band (VB) mainly comes from the V - d orbital. Remarkably, the typical multiband feature at ambient pressure is shown in Fig. S15 [30], with significant contributions from $V dz^2$ and dx^2-y^2 , $Re dz^2$ and

dx^2-y^2 orbitals around the Fermi level. With the increase of the applied pressure, the populations of electron and hole pockets changed, with hole pockets at A , L , and electron pockets between Γ - A , Γ - M , and L - H . The calculated DOSs at ambient pressure and 15 GPa are shown in Fig. 5(c). Two crossed bands near the Fermi level mainly deriving from V - $3d$, Re - $5d$, and Se - $4p$ orbitals played an essential role in the increase of electronic DOS, which was considered to facilitate the superconducting transition.

To fully comprehend the high-pressure behavior, we mapped out structural and superconducting phase diagrams of $V_{0.7}Re_{0.3}Se_2$. As shown in Fig. 5(d), room temperature resistance first decreased with pressure, where it started increasing rapidly at 30–45 GPa, and thereafter exhibited the opposite tendency as pressure increased further. The observation of the varying relationship between the upper critical field and T_c in $V_{0.7}Re_{0.3}Se_2$ might provide additional support for the pressure-driven variation of the Fermi surface [Fig. 2(e)]. In addition, the upturn in Kondo resistance moved to higher temperature with increasing pressure up to 8.7 GPa, beyond which it decreased and eventually vanished in the resistance data at 11.5 GPa. T_c increased quickly and retained a constant value of about 5.5 K, followed by a slight decrease with elevated pressure. The variation of T_c with pressure exhibited a dome-shaped superconductivity behavior. Such a P - T phase diagram of $V_{0.7}Re_{0.3}Se_2$ resembled those of unconventional superconductor cuprates [52,53] and some heavy fermion compounds [54,55].

Until now, the numerous previously reported superconducting TMDs have belonged to the single-band superconductors category. At ambient pressure, binary $1T$ - VSe_2 is an

electron-dominated single-band material [Fig. S16 [30]]. Our high-pressure work proposes the multiband superconductivity in $V_{0.7}Re_{0.3}Se_2$ compared to the parent VSe_2 under high pressure [29]. The upward curvature character $\mu_0 H_{c2}(T)$ with zero temperature in $V_{0.7}Re_{0.3}Se_2$ does not exceed the BCS paramagnetic limit. This behavior is in part quite different from that of the archetypal multigap superconductors (MgB₂ and oxypnictides) [56–59], which may be due to quite different Fermi surfaces and gap structures, especially the Fermi velocities. In this context, it should be emphasized that the difference in Fermi velocities in the two branches of $V_{0.7}Re_{0.3}Se_2$ could cause different coherence lengths in each branch, which further leads to the existence of the two-band feature in $\mu_0 H_{c2}(T)$ curves and an obvious upward positive curvature near the T_c . The Fermi velocities increase rapidly with elevated pressure while they are much slower beyond 30.0 GPa, suggesting remarkable changes in the electronic structure under pressure [Fig. 2(f)]. On the other hand, the sign change of R_H above 37.3 GPa for $V_{0.7}Re_{0.3}Se_2$ material reveals the pressure-driven Lifshitz transition while preserving $C2/m$ crystal symmetry. We thus believe that the reconstruction of the Fermi surface is triggered by the change of the dominant carriers. In contrast to binary $1T$ - VSe_2 , the reported temperature dependence of $\mu_0 H_{c2}(T)$ coincides with the isotropic single-band WHH theory, which presumes a simple spherical Fermi surface [29]. So the synergetic Re doping and pressure effect on $1T$ - VSe_2 prompt the appearance of a different superconducting state. In addition, the CDW state disappears when the Re partial substitution V, resulting in the superconducting pressure of $V_{0.7}Re_{0.3}Se_2$ being lower than that of the parent VSe_2 . With the further increase of the Re doping amount in VSe_2 , the preparation pressure of the superconducting phase in the

Re-V-Se system increases. The d -wave symmetry has been found in a limited number of compounds such as cuprates [60]. The high-pressure superconducting state of $V_{0.7}Re_{0.3}Se_2$ may be a promising candidate for a d -wave-like superconductor, which awaits in-depth research by superfluid density, scanning tunneling microscopy (STM), and angle-resolved photoemission spectroscopy (ARPES) experiments.

In conclusion, we carefully investigated the impact of high pressure on the metal $V_{0.7}Re_{0.3}Se_2$, establishing the superconducting phase diagram up to 82.1 GPa. When the Kondo effect was completely suppressed, superconductivity was observed and displayed a superconducting dome with the maximal $T_c \sim 5.5$ K at 20.9 GPa. We have discovered that the peculiar temperature dependence of the upper critical magnetic field and the nonlinear $R_{xy}(H)$ varies pointed to the multiband superconductivity character in $V_{0.7}Re_{0.3}Se_2$. Theoretical calculations proposed the main roles of V- $3d$, Re- $5d$, and Se- $4p$ orbitals in multiband superconducting states. The reconstruction of the Fermi surface resulted in the change of dominant carrier types caused by the Lifshitz transition above 37.3 GPa, which further contributed to the decrease of the T_c with increasing pressure. These results impact our knowledge about the unusual superconducting states that could be achieved by the appropriate modulations.

This work was supported by the National Key R&D Program of China (Grant No. 2022YFA1405500), National Natural Science Foundation of China (Grants No. 11974133 and No. 52072188), Program for Changjiang Scholars and Innovative Research Team in University (Grant No. IRT-15R23), and Zhejiang Provincial Science and technology innovation Team (Project No. 2021R01004).

-
- [1] H. Mukuda, M. Abe, Y. Araki, Y. Kitaoka, K. Tokiwa, T. Watanabe, A. Iyo, H. Kito, and Y. Tanaka, Uniform mixing of high- T_c superconductivity and antiferromagnetism on a single CuO_2 plane of a Hg-based five-layered cuprate, *Phys. Rev. Lett.* **96**, 087001 (2006).
- [2] X. Xi, Z. Wang, W. Zhao, J.-H. Park, K. T. Law, H. Berger, L. Forró, J. Shan, and K. F. Mak, Ising pairing in superconducting $NbSe_2$ atomic layers, *Nat. Phys.* **12**, 139 (2016).
- [3] L. Deng, T. Bontke, R. Dahal, Y. Xie, B. Gao, X. Li, K. Yin, M. Gooch, D. Rolston, T. Chen, Z. Wu, Y. Ma, P. Dai, and C. W. Chu, Pressure-induced high-temperature superconductivity retained without pressure in FeSe single crystals, *Proc. Natl. Acad. Sci. USA* **118**, e2108938118 (2021).
- [4] L. Gao, Y. Y. Xue, F. Chen, Q. Xiong, R. L. Meng, D. Ramirez, C. W. Chu, J. H. Eggert, and H. K. Mao, Superconductivity up to 164 K in $HgBa_2Ca_{m-1}Cu_mO_{2m+2+\delta}$ ($m = 1, 2$, and 3) under quasihydrostatic pressures, *Phys. Rev. B* **50**, 4260 (1994).
- [5] H. Takahashi, K. Igawa, K. Arii, Y. Kamihara, M. Hirano, and H. Hosono, Superconductivity at 43 K in an iron-based layered compound $LaO_{1-x}F_xFeAs$, *Nature (London)* **453**, 376 (2008).
- [6] W. Chen, D. V. Semenov, X. Huang, H. Shu, X. Li, D. Duan, T. Cui, and A. R. Oganov, High-temperature superconducting phases in cerium superhydride with a T_c up to 115 K below a pressure of 1 megabar, *Phys. Rev. Lett.* **127**, 117001 (2021).
- [7] A. P. Drozdov, P. P. Kong, V. S. Minkov, S. P. Besedin, M. A. Kuzovnikov, S. Mozaffari, L. Balicas, F. F. Balakirev, D. E. Graf, V. B. Prakapenka, E. Greenberg, D. A. Knyazev, M. Tkacz, and M. I. Erements, Superconductivity at 250 K in lanthanum hydride under high pressures, *Nature (London)* **569**, 528 (2019).
- [8] M. Shao, W. Chen, K. Zhang, X. Huang, and T. Cui, High-pressure synthesis of superconducting clathratelike YH_4 , *Phys. Rev. B* **104**, 174509 (2021).
- [9] F. Ke, H. Dong, Y. Chen, J. Zhang, C. Liu, J. Zhang, Y. Gan, Y. Han, Z. Chen, C. Gao, J. Wen, W. Yang, X. J. Chen, V. V. Struzhkin, H. K. Mao, and B. Chen, Decompression-driven superconductivity enhancement in In_2Se_3 , *Adv. Mater.* **29**, 1701983 (2017).
- [10] F. Hunte, J. Jaroszynski, A. Gurevich, D. C. Larbalestier, R. Jin, A. S. Sefat, M. A. McGuire, B. C. Sales, D. K. Christen, and D. Mandrus, Two-band superconductivity in $LaFeAsO_{0.89}F_{0.11}$ at very high magnetic fields, *Nature (London)* **453**, 903 (2008).
- [11] Z. Chi, X. Chen, F. Yen, F. Peng, Y. Zhou, J. Zhu, Y. Zhang, X. Liu, C. Lin, S. Chu, Y. Li, J. Zhao, T. Kagayama, Y. Ma, and Z. Yang, Superconductivity in pristine $2H_4$ - MoS_2 at ultrahigh pressure, *Phys. Rev. Lett.* **120**, 037002 (2018).

- [12] T. V. Bay, T. Naka, Y. K. Huang, H. Luigjes, M. S. Golden, and A. de Visser, Superconductivity in the doped topological insulator $\text{Cu}_x\text{Bi}_2\text{Se}_3$ under high pressure, *Phys. Rev. Lett.* **108**, 057001 (2012).
- [13] C. C. Tsuei and J. R. Kirtley, Pairing symmetry in cuprate superconductors, *Rev. Mod. Phys.* **72**, 969 (2000).
- [14] J. Nagamatsu, N. Nakagawa, T. Muranaka, Y. Zenitani, and J. Akimitsu, Superconductivity at 39 K in magnesium diboride, *Nature (London)* **410**, 63 (2001).
- [15] P. M. Shirage, K. Kihou, K. Miyazawa, C. H. Lee, H. Kito, H. Eisaki, T. Yanagisawa, Y. Tanaka, and A. Iyo, Inverse iron isotope effect on the transition temperature of the $(\text{Ba}, \text{K})\text{Fe}_2\text{As}_2$ superconductor, *Phys. Rev. Lett.* **103**, 257003 (2009).
- [16] S. Medvedev, T. M. McQueen, I. A. Troyan, T. Palasyuk, M. I. Erements, R. J. Cava, S. Naghavi, F. Casper, V. Ksenofontov, G. Wortmann, and C. Felser, Electronic and magnetic phase diagram of $\beta\text{-Fe}_{1.01}\text{Se}$ with superconductivity at 36.7 K under pressure, *Nat. Mater.* **8**, 630 (2009).
- [17] H. Q. Yuan, F. M. Grosche, M. Deppe, C. Geibel, G. Sparn, and F. Steglich, Observation of two distinct superconducting phases in CeCu_2Si_2 , *Science* **302**, 2104 (2003).
- [18] X. J. Chen, V. V. Struzhkin, Y. Yu, A. F. Goncharov, C. T. Lin, H. K. Mao, and R. J. Hemley, Enhancement of superconductivity by pressure-driven competition in electronic order, *Nature (London)* **466**, 950 (2010).
- [19] L. Sun, X. J. Chen, J. Guo, P. Gao, Q. Z. Huang, H. Wang, M. Fang, X. Chen, G. Chen, Q. Wu, C. Zhang, D. Gu, X. Dong, L. Wang, K. Yang, A. Li, X. Dai, H. K. Mao, and Z. Zhao, Re-emerging superconductivity at 48 kelvin in iron chalcogenides, *Nature (London)* **483**, 67 (2012).
- [20] K. Jin, N. P. Butch, K. Kirshenbaum, J. Paglione, and R. L. Greene, Link between spin fluctuations and electron pairing in copper oxide superconductors, *Nature (London)* **476**, 73 (2011).
- [21] M.-H. Fang, H.-D. Wang, C.-H. Dong, Z.-J. Li, C.-M. Feng, J. Chen, and H. Q. Yuan, Fe-based superconductivity with $T_c = 31$ K bordering an antiferromagnetic insulator in $(\text{Ti}, \text{K})\text{Fe}_x\text{Se}_2$, *Europhys. Lett.* **94**, 27009 (2011).
- [22] M. Hücker, M. v. Zimmermann, G. D. Gu, Z. J. Xu, J. S. Wen, G. Xu, H. J. Kang, A. Zheludev, and J. M. Tranquada, Stripe order in superconducting $\text{La}_{2-x}\text{Ba}_x\text{CuO}_4$ ($0.095 \leq x \leq 0.155$), *Phys. Rev. B* **83**, 104506 (2011).
- [23] J. P. Sun, P. Shahi, H. X. Zhou, Y. L. Huang, K. Y. Chen, B. S. Wang, S. L. Ni, N. N. Li, K. Zhang, W. G. Yang, Y. Uwatoko, G. Xing, J. Sun, D. J. Singh, K. Jin, F. Zhou, G. M. Zhang, X. L. Dong, Z. X. Zhao, and J. G. Cheng, Reemergence of high- T_c superconductivity in the $(\text{Li}_{1-x}\text{Fe}_x)\text{OHFe}_{1-y}\text{Se}$ under high pressure, *Nat. Commun.* **9**, 380 (2018).
- [24] F. H. Yu, T. Wu, Z. Y. Wang, B. Lei, W. Z. Zhuo, J. J. Ying, and X. H. Chen, Concurrence of anomalous Hall effect and charge density wave in a superconducting topological kagome metal, *Phys. Rev. B* **104**, L041103 (2021).
- [25] C. Tian, Y. Gao, X. Huang, Y. Fang, F. Huang, and T. Cui, Giant reduction of stabilized pressure for the superconducting $\text{Re}_{0.8}\text{V}_{0.2}\text{Se}_2$ phase, *Inorg. Chem.* **62**, 11626 (2023).
- [26] S. Xu, Z. Liu, P. Yang, K. Chen, J. Sun, J. Dai, Y. Yin, F. Hong, X. Yu, M. Xue, J. Gouchi, Y. Uwatoko, B. Wang, and J. Cheng, Superconducting phase diagrams of S-doped 2H-TaSe₂ under hydrostatic pressure, *Phys. Rev. B* **102**, 184511 (2020).
- [27] C. Tian, Y. Gao, F. Tian, X. Wang, Z. Zhang, D. Duan, X. Huang, and T. Cui, Dimensionality switching and superconductivity transition in dense 1T-HfSe₂, *Phys. Rev. B* **105**, L180506 (2022).
- [28] Q. Niu, W. Zhang, Y. T. Chan, E. C. T. O'Farrell, R. Doganov, K. Y. Yip, K. T. Lai, W. C. Yu, B. Özyilmaz, G. R. Stewart, J. S. Kim, and S. K. Goh, Stabilization of antiferromagnetism in 1T-Fe_{0.05}TaS₂, *Phys. Rev. Res.* **2**, 023297 (2020).
- [29] S. Sahoo, U. Dutta, L. Harnagea, A. K. Sood, and S. Karmakar, Pressure-induced suppression of charge density wave and emergence of superconductivity in 1T-VSe₂, *Phys. Rev. B* **101**, 014514 (2020).
- [30] See Supplemental Material at <http://link.aps.org/supplemental/10.1103/PhysRevB.108.L180507> for detailed experimental and computational methods, data pertaining to high-pressure electrical resistance measurements, synchrotron XRD analysis, and calculations of the band structure of, which includes Refs. [31–40].
- [31] H. K. Mao, J. Xu, and P. M. Bell, Calibration of the ruby pressure gauge to 800 kbar under quasi-hydrostatic conditions, *J. Geophys. Res.* **91**, 4673 (1986).
- [32] Y. Akahama and H. Kawamura, Pressure calibration of diamond anvil Raman gauge to 410 GPa, *J. Phys. Conf. Ser.* **215**, 012195 (2010).
- [33] L. J. Van der Pauw, A method of measuring the resistivity and Hall coefficient on lamellae of arbitrary shape, *Philips Tech. Rev.* **20**, 220 (1958).
- [34] N. Ni, J. M. Allred, B. C. Chan, and R. J. Cava, High T_c electron doped $\text{Ca}_{10}(\text{Pt}_3\text{As}_8)(\text{Fe}_2\text{As}_2)_5$ and $\text{Ca}_{10}(\text{Pt}_4\text{As}_8)(\text{Fe}_2\text{As}_2)_5$ superconductors with skutterudite intermediary layers, *Proc. Natl. Acad. Sci. USA* **108**, E1019 (2011).
- [35] C. Prescher and V. B. Prakapenka, DIOPTAS: A program for reduction of two-dimensional X-ray diffraction data and data exploration, *High Press. Res.* **35**, 223 (2015).
- [36] H. M. Rietveld, A profile refinement method for nuclear and magnetic structures, *J. Appl. Crystallogr.* **2**, 65 (1969).
- [37] G. Kresse and D. Joubert, From ultrasoft pseudopotentials to the projector augmented-wave method, *Phys. Rev. B* **59**, 1758 (1999).
- [38] G. Kresse and J. Furthmüller, Efficiency of *ab-initio* total energy calculations for metals and semiconductors using a plane-wave basis set, *Comput. Mater. Sci.* **6**, 15 (1996).
- [39] J. P. Perdew, K. Burke, and M. Ernzerhof, Generalized gradient approximation made simple, *Phys. Rev. Lett.* **77**, 3865 (1996).
- [40] H. J. Monkhorst and J. D. Pack, Special points for Brillouin-zone integrations, *Phys. Rev. B* **13**, 5188 (1976).
- [41] N. R. Werthamer, E. Helfand, and P. C. Hohenberg, Temperature and purity dependence of the superconducting critical field, H_{c2} . III. electron spin and spin-orbit effects, *Phys. Rev.* **147**, 295 (1966).
- [42] M. Li, K. Xu, M. Xu, Y. Fang, Z. Yan, N. Li, Z. Yu, J. Zhang, C. Kenney-Benson, X. Wang, and L. Wang, Pressure-induced electronic anomaly and multiband superconductivity in the doped topological insulator $\text{Nb}_x\text{Bi}_2\text{Se}_3$, *Phys. Rev. B* **100**, 224521 (2019).
- [43] S. Ran, C. Eckberg, Q. P. Ding, Y. Furukawa, T. Metz, S. R. Saha, I. L. Liu, M. Zic, H. Kim, J. Paglione, and N. P. Butch, Nearly ferromagnetic spin-triplet superconductivity, *Science* **365**, 684 (2019).
- [44] J. Jaroszynski, S. C. Riggs, F. Hunte, A. Gurevich, D. C. Larbalestier, G. S. Boebinger, F. F. Balakirev, A. Migliori,

- Z. A. Ren, W. Lu, J. Yang, X. L. Shen, X. L. Dong, Z. X. Zhao, R. Jin, A. S. Sefat, M. A. McGuire, B. C. Sales, D. K. Christen, and D. Mandrus, Comparative high-field magnetotransport of the oxypnictide superconductors $R\text{FeAsO}_{1-x}\text{F}_x$ ($R = \text{La}, \text{Nd}$) and $\text{SmFeAsO}_{1-\delta}$, *Phys. Rev. B* **78**, 064511 (2008).
- [45] H. Suderow, V. G. Tissen, J. P. Brison, J. L. Martínez, S. Vieira, P. Lejay, S. Lee, and S. Tajima, Pressure dependence of the upper critical field of MgB_2 and of $\text{YNi}_2\text{B}_2\text{C}$, *Phys. Rev. B* **70**, 134518 (2004).
- [46] U. S. Kaluarachchi, V. Taufour, A. E. Böhmer, M. A. Tanatar, S. L. Bud'ko, V. G. Kogan, R. Prozorov, and P. C. Canfield, Nonmonotonic pressure evolution of the upper critical field in superconducting FeSe, *Phys. Rev. B* **93**, 064503 (2016).
- [47] K. Scharnberg and R. A. Klemm, p -wave superconductors in magnetic fields, *Phys. Rev. B* **22**, 5233 (1980).
- [48] V. G. Kogan and R. Prozorov, Orbital upper critical field and its anisotropy of clean one- and two-band superconductors, *Rep. Prog. Phys.* **75**, 114502 (2012).
- [49] K. Kirshenbaum, P. S. Syers, A. P. Hope, N. P. Butch, J. R. Jeffries, S. T. Weir, J. J. Hamlin, M. B. Maple, Y. K. Vohra, and J. Paglione, Pressure-induced unconventional superconducting phase in the topological insulator Bi_2Se_3 , *Phys. Rev. Lett.* **111**, 087001 (2013).
- [50] J. Bardeen, L. N. Cooper, and J. R. Schrieffer, Theory of superconductivity, *Phys. Rev.* **108**, 1175 (1957).
- [51] F. Birch, Finite elastic strain of cubic crystals, *Phys. Rev.* **71**, 809 (1947).
- [52] N. Doiron-Leyraud, C. Proust, D. LeBoeuf, J. Levallois, J. B. Bonnemaïson, R. Liang, D. A. Bonn, W. N. Hardy, and L. Taillefer, Quantum oscillations and the Fermi surface in an underdoped high- T_c superconductor, *Nature (London)* **447**, 565 (2007).
- [53] P. A. Lee, N. Nagaosa, and X.-G. Wen, Doping a Mott insulator: Physics of high-temperature superconductivity, *Rev. Mod. Phys.* **78**, 17 (2006).
- [54] V. A. Sidorov, M. Nicklas, P. G. Pagliuso, J. L. Sarrao, Y. Bang, A. V. Balatsky, and J. D. Thompson, Superconductivity and quantum criticality in CeCoIn_5 , *Phys. Rev. Lett.* **89**, 157004 (2002).
- [55] P. Gegenwart, Q. Si, and F. Steglich, Quantum criticality in heavy-fermion metals, *Nat. Phys.* **4**, 186 (2008).
- [56] A. Gurevich, Limits of the upper critical field in dirty two-gap superconductors, *Physica C (Amsterdam, Neth.)* **456**, 160 (2007).
- [57] A. Y. Liu, I. I. Mazin, and J. Kortus, Beyond Eliashberg superconductivity in MgB_2 : Anharmonicity, two-phonon scattering, and multiple gaps, *Phys. Rev. Lett.* **87**, 087005 (2001).
- [58] I. I. Mazin, D. J. Singh, M. D. Johannes, and M. H. Du, Unconventional superconductivity with a sign reversal in the order parameter of $\text{LaFeAsO}_{1-x}\text{F}_x$, *Phys. Rev. Lett.* **101**, 057003 (2008).
- [59] K. Kuroki, S. Onari, R. Arita, H. Usui, Y. Tanaka, H. Kontani, and H. Aoki, Unconventional pairing originating from the disconnected Fermi surfaces of superconducting $\text{LaFeAsO}_{1-x}\text{F}_x$, *Phys. Rev. Lett.* **101**, 087004 (2008).
- [60] T. Valla, A. V. Fedorov, J. Lee, J. C. Davis, and G. D. Gu, The ground state of the pseudogap in cuprate superconductors, *Science* **314**, 1914 (2006).